Design and Implementation of OPU-based Laser Direct Writing Lithography System

Binchao Wang, Zixiao Yu, Hongxia Bian, Yanjun Cui, and Peng Tu*

College of Science, Gansu Agricultural University, Lanzhou, 730070, PR China
**Corresponding author's e-mail: tupeng815@163.com*

Laser direct writing is a promising technology for flexible electronics, microsensors, and microfluidic chips. In this study, we propose a low-cost micro and nano lithography process using near-field laser direct writing. Our platform achieves a high print resolution of 3.96 µm for photosensitive resin, which is better than that of common commercial 3D printing devices. We adjust the laser power and scanning speed to precisely control the print resolution from 3.96 µm to 55.94 µm. The lithography system demonstrates repeatability and stability in repeated experiments, and wide format printing (20×20 mm) shows its ability to print across scales. Our approach employs an inexpensive photohead picker OPU, which costs less than ten dollars, to meet the demand for small-volume, low-cost, multi-scale micro and nano device manufacturing.

DOI: 10.2961/jlmn.2024.01.2004
Keywords: direct laser writing, laser power, scanning speed, resolution

1. Introduction

The optical projection lithography system is widely used in micro- and nano-fabrication due to its ability to project a mask pattern onto photoresist with advanced optical design, ensuring good repeatability and large-area fabrication. However, the prefabricated physical mask version results in long development and production cycles, limited resolution due to the diffraction limit of the mask and wavelength, and increasing mask costs with higher resolutions[1]. The development of maskless, low-cost, and high-resolution lithography systems is therefore a pressing issue in micro- and nano-structure fabrication. Guo et al.[2] proposed surface plasmon resonance interferometric nanolithography for producing fine patterns that exceed diffraction limits. Merkininkait et al.[3] use multi-photon lithography and thermal post-processing technology to achieve the inorganic three-dimensional field for the manufacture of high-precision, high-temperature and corrosion-resistant micro-nano devices. Although ion beam[4] and electron beam[5] lithography can achieve feature sizes of tens of nanometers, their high complexity and cost limit their application.

Laser direct writing (LDW) changes the physical state and properties of materials by absorbing laser energy, enabling flexible one-step micromachining of two- or three-dimensional structures[6]. This method offers short processing cycles, low temperatures, scalability, a wide range of applicable materials, and low environmental requirements[7]. LDW has been widely used to fabricate microelectrodes[8–13], microfluidic devices[14], electric heaters[15], sensor devices[16–21], supercapacitors[22], and flexible displays[23], significantly reducing manufacturing and equipment costs. However, the laser light sources often used in LDW devices are high-power femtosecond[24] or picosecond lasers[25], which are expensive and not affordable for all experimental groups. Consequently, there is a dire need for low-cost, maskless laser direct writing devices.

In recent years, continuous wave lasers have emerged as a promising and cost-effective technology for sub-micron lithography. Various low-cost solutions based on semiconductor diode lasers have been proposed. Mueller et al.[26] used a relatively inexpensive CW 405 nm diode pulsed laser to achieve high resolution stereolithography at the submicron level. Hautefeuille et al.[27] propose a simple and inexpensive alternative to high-power lasers for direct fabrication of microchannels and rapid prototyping of polydimethylsiloxanes. However, achieving high print resolution remains a challenge for building low-cost direct writing lithography equipment. Continuous wave laser direct writing systems have shown promise in achieving feature resolutions of up to 0.5-1 µm by adjusting the laser wavelength and focus position[28]. Nonetheless, continuous wave lasers typically require complex optical path systems to achieve higher resolution and manufacturing accuracy, and high-precision optical equipment can be expensive.

Optical Pick-up Unit(OPU) from optical drive recorders provide an affordable alternative for continuous wave micro-lithography and nano-lithography by using low-power continuous wave diodes as the light source with optical limit diffraction devices. For example, Rothenbach et al.[29] achieved sub-micron (450 nm) lithography on standard SU-8 photoresists using an OPU from a blue light driver in a lithography system. Hwu et al.[30] used a mass-produced OPU as a light source for photopolymerization 3D printing and demonstrated finely tunable diode lasers that can adjust the print resolution from tens of microns to hundreds of nanometers, enabling affordable high-resolution micro- and nano-3D printing. These findings pave the way for simple and cost-effective rapid manufacturing.

Based on this, the OPU was selected as the optical path system and a diode laser from the laser readhead was used as the laser light source to develop a low-cost continuous wave laser direct writing platform. The cost of the platform is almost negligible compared to the cost of digital masks and femtosecond lasers. The process enables three-dimensional lithography by precisely controlling the laser power and beam waist position. The lithography system can change the laser wavelength by replacing the laser diode, or the laser readhead can be replaced as a component. Multiple OPU can also be used to form an array of laser readheads. With the ability to customise microstructures quickly and flexibly, the system shows a promising future in the manufacturing of small volume, low-cost, multi-spec micro and nano devices.

2. Platform construction and commissioning

2.1 Optical Head Picker OPU as a Light Source

To develop a lithography platform, the OPU is utilized as an economical option that offers a diode laser light source and compact diffraction-limited optics. This includes high-precision positioning and multi-wavelength laser modes. The OPU, sourced from optical disc drivers, is considered a practical approach to improve lithography resolution. It allows for easy adjustment of print resolutions from tens of microns to hundreds of nanometer without the need for costly lasers or complex optical path systems[31].

2.2 Construction of the OPU direct lithography system

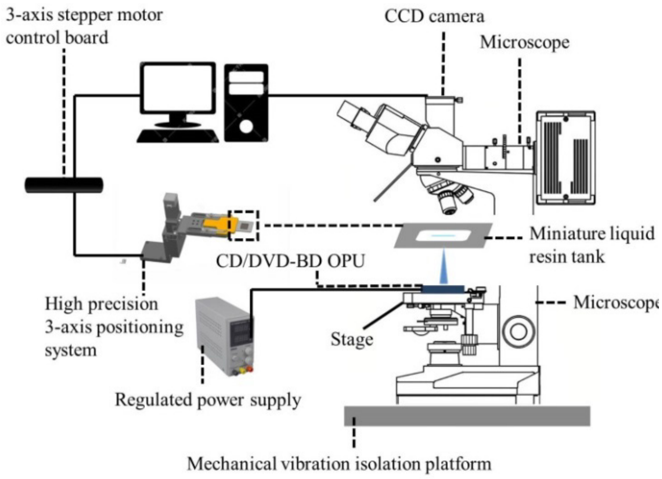

Fig. 1 OPU direct lithography system

The laser lithography system comprises a CD/DVD-BD OPU, a mechanical vibration isolation platform, a miniature liquid resin tank, a high precision 3-axis positioning system, a miniature stepper electrode driver, a 3-axis stepper motor control board, and a DC regulated power supply. The three-axis positioning stage is composed of three linear stages, namely XYZ. The XY-axis positioning stage is employed to achieve the scanning motion of the laser spot at the bottom of the resin tank in Fig. 1.

To drive the XYZ linear stages, the lithography system utilizes three miniature stepper motors, capable of attaining a maximum of 256 subdivisional microsteps, where each subdivisional microstep corresponds to a minimum linear stage movement distance of 19.5 nm. The screw pitch of the individual linear stage is 1 mm, and for every 256 subdivisional microsteps, the motor turns the step angle by 1.8°, and the stage moves by 5 μm, with a maximum movement distance of 25 mm in the XYZ direction. The DC regulated power supply precisely controls the laser diode power and can drive the voice coil motor. The trough is mounted on the slide fixture of the Z-axis stage, as illustrated in Fig. 2.

To cure the photosensitive resin on the desired substrate, the desired pattern is converted into G-code, and the code commands are transmitted to the motors to drive the X and Y linear stages in a scanning motion, thereby achieving the laser dotted line drawing action. The system uses an inverted lithography design, with the OPU mounted on a microscope stage, focusing the laser on the top of the objective lens, and enabling real-time observation of the print from the top, utilizing an optical microscope equipped with a high-resolution CCD. The small footprint of the system makes it suitable for any experimental environment.

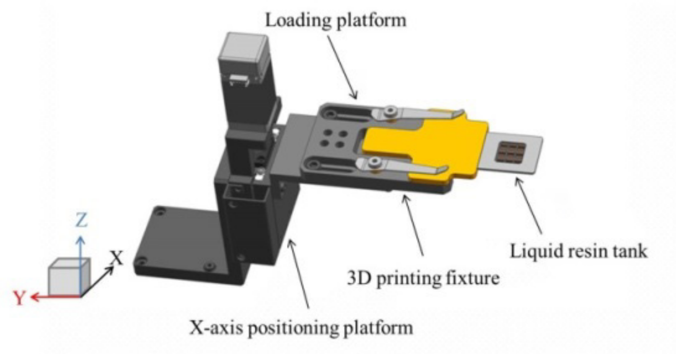

Fig. 2 Removable carrier table and liquid resin tank

The photosensitive resin was poured into the miniature liquid resin tank, and the bath was mounted on the XYZ positioning stage of the lithography system. The laser power and beam waist position were adjusted to optimise the curing of the photosensitive resin. The system was then used to print various microstructures, including lines, circles, and complex patterns,with different feature sizes and line widths ranging from tens of micrometer to a few hundred nanometer. The print quality was evaluated using an optical microscope equipped with a high-resolution CCD camera.

2.3 Leveling and focusing

When using the Z-axis platform for the first time, it is necessary to adjust its position so that the bottom of the trough is in clear focus under the microscope. The laser focus size at the bottom of the trough is then characterized with the aid of the microscope, and the coarse and fine focus knobs of the microscope are adjusted to achieve the desired focus. The coarse focus knob moves the stage 40 mm in one turn, while the fine focus knob moves it 0.2 mm in one turn. The knob is subdivided 200 times in one turn, providing a height adjustment resolution of 1 μm. Finally, the voice coil motor is adjusted to focus the laser on the bottom of the photosensitive resin trough. The voice coil motor is controlled by a DC regulated power supply of 1 to 2 V, and can be adjusted with positive or negative voltage to achieve a positioning accuracy of 1 mV/μm.

To ensure that the laser spot remains consistent in size at all points on the bottom of the trough, the photosensitive resin trough must be leveled before printing. This can be achieved by adjusting the vibration isolation to horizontal and then leveling the slide fixture and microscope stage with a level. The Z-axis positioning stage is then moved to the desired height, and the microscope is used to observe the solid-liquid partition in the resin bath until a clear image can be observed within the X- and Y-axis travel of the positioning stage. The OPU diode laser power supply is switched on and the linear stage is moved in the X and Y directions to confirm that the laser focal spot remains at the correct size at each point on the substrate. By scanning the X and Y linear stages and adjusting the height of the Z-axis stage, it can be ensured that the plane of the substrate and the plane of focus of the laser beam coincide.

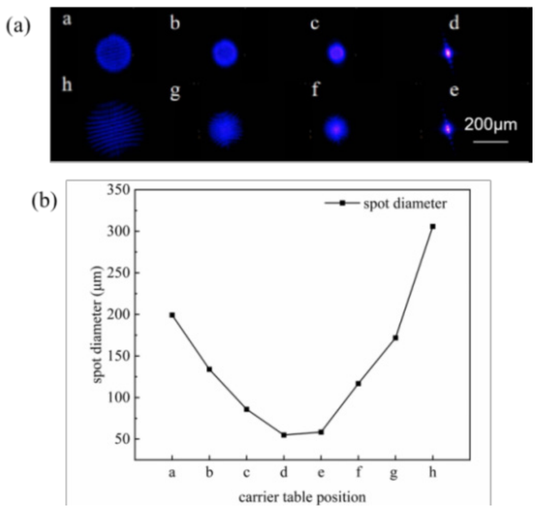

Fig. 3 Light spot size at different height of carrier table (a)light spot images (b) light spot diameter

Fig. 3(a) shows that the OPU was placed on the microscope stage, and the height of the stage was adjusted from point a to point h in turn to obtain spot images of different sizes. As shown in Fig. 3(b), the spot focus size tends to decrease and then increase as the height increases, and the light intensity distribution shows the typical characteristics of a Gaussian beam, with the spot at point d being the smallest at 54.98 μm. The optimum working distance from the objective assembly of the OPU to the bottom of the trough is determined by adjusting the position of the laser along the Z-axis, and the ideal working distance needs to be adjusted within a range of less than 2 mm.

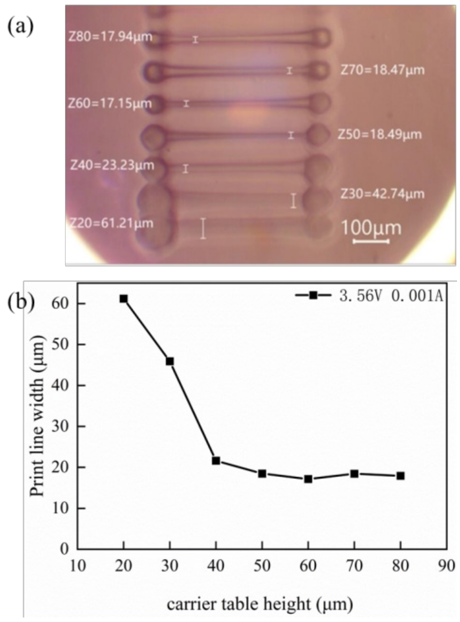

Fig. 4 Microlines based on photopolymerization (a) printed line widths at different height (b) variation of line width with height

The adjustment of the carrier table height is crucial for obtaining the minimum print line width. The carrier table was adjusted from position c to e in Fig. 3(a) and the relationship between the height of the carrier table and the print line width was analyzed, which was an important step in the commissioning of the platform. Fig. 4(a) shows that eight straight lines were solidified from Z20 to Z80, with a significant decrease in print line width from 61.21 μm to 23.23 μm during the stage from Z20 to Z40. The decrease in print line width was caused by the gradual upward movement of the laser spot near the bottom of the trough as the carrier table height was increased. The print line width remained stable within the height range from Z40 to Z80, indicating that the Z40-Z80 interval is a suitable working height range. The laser spot size remained constant during the rise from point d to point e, resulting in an average line width diameter of 18.74 μm. The print line width was approximately 33.05% of the spot diameter due to the insufficient energy of the laser beam at the edge of the beam to cure the photosensitive resin, resulting in a narrower cured line width than the laser spot diameter. It was observed from Fig. 4(a) that the cured line was wide at both ends and narrow in the middle, which was caused by the initial acceleration and deceleration at the end of the positioning stage movement. To minimize this effect, the positioning stage should be kept moving at a constant speed as much as possible in subsequent tests.

2.4 Regulation of laser power and scanning speed

The laser power is regulated by adjusting the voltage and current of the DC voltage regulator. A G-code is created to regulate the movement speed of the positioning platform, achieving different speeds of laser scanning of the photosensitive resin. The designed path code is then transmitted to the printing device. The laser beam operates similarly to the nozzle in FDM (Fused Deposition Modelling). The scanning speed of the laser is set at 0-50 mm/min, and this parameter also determines the exposure time. When using a 405 nm diode, the drive current of 40 mA can output over 100 mW. To ensure a longer laser life and better lithography performance, a drive current of less than 20 mA and a laser power of up to 50 mW is typically used without modifying the thermal conditions of the optical readhead. Laser direct writing systems can easily replace the laser diode, allowing for the alteration of the laser wavelength.

Different laser diodes with varying wavelengths can be used depending on the material being printed. For instance, a 355 nm laser diode can be used for printing on materials such as glass, while a 532 nm laser diode can be used for printing on metal. The selection of the laser diode should be based on the absorption characteristics of the photosensitive material to ensure the best lithography performance. The laser power and scanning speed can be adjusted according to the requirements of the printing process to achieve the desired exposure time and resolution. The use of laser direct writing systems has significantly expanded the range of materials that can be used in additive manufacturing, allowing for the creation of complex structures with high precision.

3. Printing tests

The size of the cured region in the liquid resin is directly related to the local laser exposure energy, which is determined by the scanning speed and laser power. By adjusting these parameters, the local laser exposure can be precisely controlled, enabling the production of structures with a precise and consistent print line width. This is an important aspect of laser direct writing, as it allows for the creation of complex and precise structures with high resolution and accuracy.

3.1 Effect of scanning speed on print line width

The laser diode was operated at 3.86 V and a current of 0.006 A. Various scanning speeds were employed to expose the photoresist, resulting in 11 printed lines on the coverslip as shown in Fig. 5. It was observed that as the scanning speed increased from 2 mm/min to 22 mm/min, the width of the printed lines decreased from 55.41 μm to 3.96 μm. The smaller print line width was due to reduced local exposure resulting from the higher scanning speed, and was negatively correlated with the scanning speed. When the scanning speed exceeded 14 mm/min, periodic fluctuations in the laser trajectory were observed, with an amplitude of approximately 5 μm. The printing accuracy of the system was not only affected by the printing process, but also by other factors influencing the distribution of laser energy, such as plastic deformation, scratches, surface flatness of the sample, surface stains, and parallelism of the substrate to the objective.

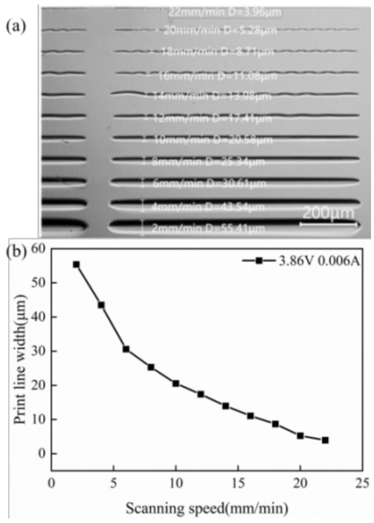

Fig. 5 Print line widths at different scanning speeds

3.2 Effect of laser power on print line width

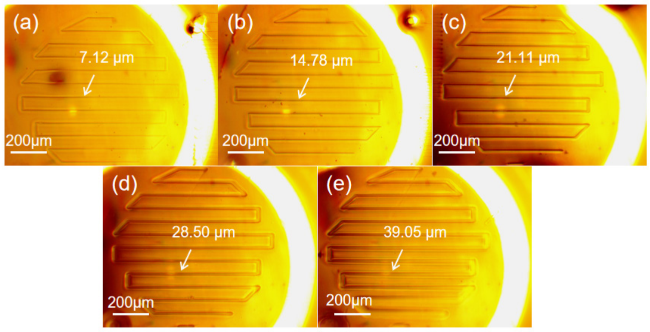

Fig. 6 Optical microscope images at different laser powers (a-e) Laser powers of 23.16mW, 34.92mW, 47.16mW, 60.15mW, 73.26mW, respectively

Fig. 6 shows the bow pattern printed at a scanning speed of 20 mm/min and various laser powers, resulting in a line width of 7.12 μm at 23.16 mW and 39.05 μm at 73.26 mW. The data suggest a strong correlation between the laser power and print line width, with higher laser powers leading to smaller line widths. The system exhibits excellent printing accuracy and repeatability, with patterns printed multiple times that are evenly distributed and well-positioned. The theoretical voxel widths in Table 1 were calculated based on these results. The print line width (d) is linearly related to the laser power (A), which is formulated as

$$d = -7.439 + 0.619A(R^2 = 0.994) \qquad (1)$$

providing useful information for optimizing the printing process.

Table 1 Print line widths at different laser powers

Laser power(mW)	23.16	34.92	47.16	60.15	73.26
Print line width(μm)	7.12	14.78	21.11	28.5	39.05

3.3 Methods for precisely tuning the print resolution

The print line widths obtained by scribing on the coverslips at different scanning speeds and laser powers are presented in Fig. 7. At the same power level, the line width decreases with increasing scan speed until it cannot be printed, and this trend is observed for multiple laser powers. On the other hand, at the same scan speed, the print line width increases with increasing laser power. When the laser power is too low or the scanning speed is too fast, the local exposure threshold is not reached, leading to no photopolymerization, which is consistent with theoretical predictions. For instance, a laser power of 19.05 mW at a scanning speed of 22 mm/min yields a minimum line width of 3.96 µm, while a laser power of 23.16 mW at a scanning speed of 2 mm/min results in a maximum line width of 55.94 µm. These values can be further adjusted by increasing the laser power or reducing the scanning speed to enhance the print line width size and increase the printing efficiency. However, it is important to note that increasing laser power and decreasing scanning speed may result in trade-offs in print quality, accuracy, and overall printing time. Therefore, it is crucial to carefully balance these factors when optimizing printing parameters for a specific application. Additionally, other factors such as material properties and substrate characteristics can also influence printing performance and should be taken into consideration.

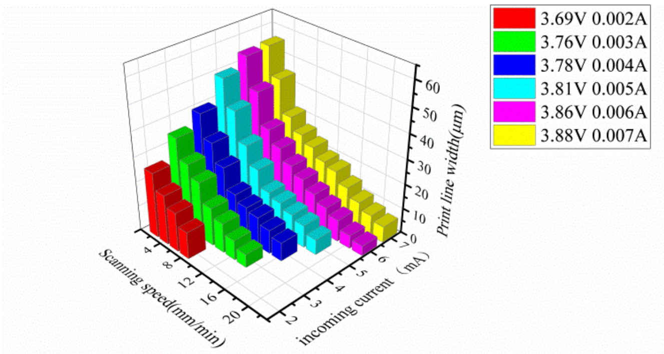

Fig. 7 Line widths at different scanning speeds and laser powers

To investigate the impact of scanning speed and laser power on resolution, we examined the relationship between exposure time and exposure volume in Fig. 8. Microdot arrays were generated using a laser operating voltage of 3.91 V and operating current of 11 mA, with exposure durations of 80 ms, 160 ms, 320 ms, and 640 ms. The average diameter of the printed dots were 7.78 µm, 10.16 µm, 12.14 µm, and 13.61 µm for exposure durations of 80 ms, 160 ms, 320 ms, and 640 ms, respectively. After multiple exposures in the central area, the dot diameter increased to 27.96 µm. Fig. 8(b) demonstrates that the diameter of the printed dots increases with increasing exposure time, which is attributed to the heightened local exposure.

The exposure time affects the exposure volume, which in turn affects the diameter of the printed dots. As the exposure time increases, more photons are absorbed by the photoresist, resulting in a larger photopolymerisation reaction and hence a larger diameter of the printed dots. The result is consistent with the theory that the exposure time has a direct effect on the photopolymerisation process.

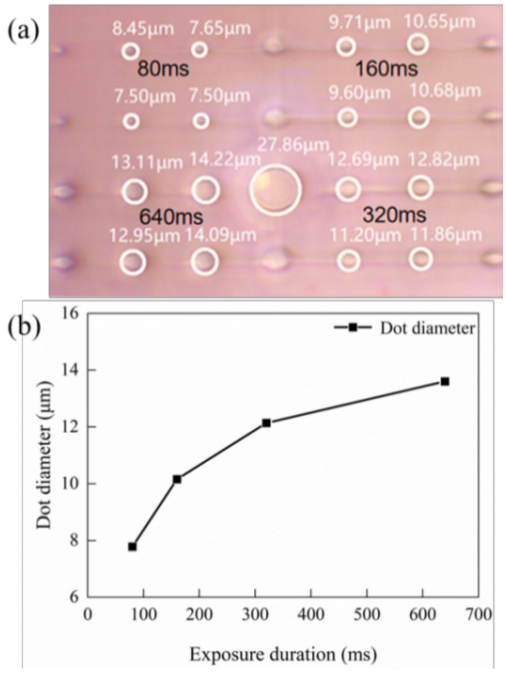

Fig. 8 Dots based on photopolymerisation reactions at different exposure times (a) Diameter of dots at exposure times of 80 ms, 160 ms, 320 ms and 640 ms (b) Variation of dot diameter with exposure time

The resolution of 3D printing is determined by the size of the voxel, which is the smallest unit of material that can be printed in 3D. In laser-based 3D printing methods, such as stereolithography (SLA), a low power continuous wave laser is used to selectively cure a liquid photopolymer into a solid structure. The laser light is highly focused and directed by a series of mirrors to scan the surface of the liquid photopolymer layer by layer, curing the material at the desired locations. The size of the cured voxel is determined by the laser energy and the optical properties of the photopolymer. By controlling the laser energy and the scanning pattern, it is possible to achieve high-resolution 3D prints with fine details and smooth surface finish.The laser energy during this process affects the size of the cured voxel and the voxel width V_W is defined as[32]

$$V_W = W_0 \sqrt{2 \ln\left(\frac{E_0}{E_C}\right)} \qquad (2)$$

Where E_0 is the laser intensity at the surface of the photopolymer, E_C is the critical exposure energy to start photopolymerisation, W_0 is the radius of the beam and W_0 is proportional to V_W. Therefore reducing the beam focus size during photopolymerisation will significantly improve the print resolution. The laser spot radius W_0 is defined as

$$W_0 = \frac{4\lambda f M^2}{\pi D} \qquad (3)$$

where λ is the wavelength of the laser, f is the focal length of the lens, D is the diameter of the input beam at the lens and M^2 is the beam quality of the laser. The theoretical voxel width of the 405 nm blue OPU is calculated using the formula for the laser spot radius W_0, which takes into account the wavelength of the laser, the focal length of the lens, the diameter of the input beam at the lens, and the beam quality of the laser. In this study, the KEM410 blue OPU has an objective lens NA of 0.65, an aperture of 3 mm and a beam quality of around 1.2, which are used to calculate the theoretical voxel widths in Table 2. The actual print line widths are close to the theoretical voxel widths with a relative error of 0.52%, which confirms the consistency of the experimental results with theory.

Table 2 Voxel widths and actual print line widths at different laser powers

Laser power （mW）	7.38	11.28	15.12	19.05	23.16	27.16
Theoretical voxel width （μm）	16.81	26.93	33.81	39.34	44.05	47.81
Print line width （μm）	20.05	27.71	31.66	40.12	43.54	44.60

3.4 Wide format complex pattern printing

After achieving precise control of the print size, more complex patterns were attempted, printing the Gansu 1
Agricultural University emblem and animal patterns respectively within less than 5 mm in Fig. 9.

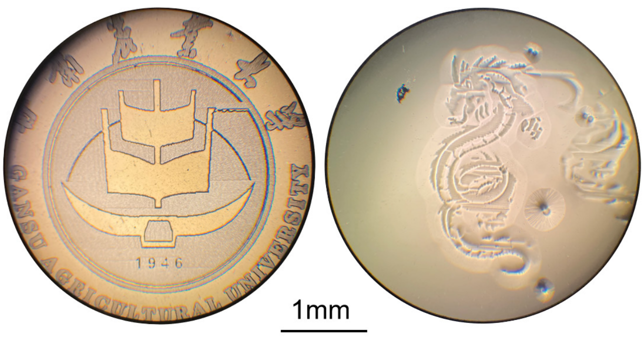

Fig. 9 School logo and animal design printed on laser lithography platform

The results showed that the platform was capable of producing high-quality microstructures with resolutions down to a few mocrometres. The print speed was found to be mainly limited by the speed of the XYZ positioning stage and the curing time of the photosensitive resin. The authors suggest that further improvements could be made to the platform to increase the print speed and to extend the range of materials that can be used. Overall, the platform offers a low-cost and flexible solution for micro- and nanofabrication that could be used in a wide range of applications, including photonics, microfluidics, and biosensors.

4. Conclusion

The paper presents a novel approach to micro-nano lithography using a low-cost, near-field laser direct writing method. We built a platform capable of achieving a print resolution of 3.96 μm, which is better than that of commercial 3D printing devices. We optimized the printing scheme and evaluated the print quality using a 405 nm laser cross-linked cured photosensitive resin provided by OPU, which triggers non-linear photopolymerization of the photopolymer by laser scanning. We discuss the effects of laser power, laser scanning speed, and local exposure on print resolution, providing an effective method for precise control of print resolution. We confirm that the OPU, which is inexpensive and has a closed-loop control system, is capable of micron-level printing and can meet the growing demand for the development of flexible micro-devices. The proposed process has promising applications for the future fabrication of low-volume, low-cost, multi-spec micro and nano devices.

Acknowledgments

The authors gratefully acknowledge the support from the Natural Science Foundation of Gansu Province under Grant No. 22JR5RA866, the Open Recruitment of Doctoral Research Start-up Fund of Gansu Agricultural University under Grant No. GAU-KYQD-2019-24, and the Natural Science Basic Research Program of Shanxi Province under Grant No. 2020JQ-119.

References

[1] A. Grushina: Adv. Opt. Technol., 8, (2019) 163.
[2] X. Luo and T. Ishihara: Appl. Phys. Lett., 84, (2004) 4780.
[3] G. Merkininkaitė, E. Aleksandravičius, M. Malinauskas, D. Gailevičius, and S. Šakirzanovas: Optoelectron Adv, 5, (2022) 210077.
[4] A. Zoubir, C. Lopez, M. Richardson, and K. Richardson: Opt. Lett., 29, (2004) 1840.
[5] M. Malinauskas, P. Danilevicius, and S. Juodkazis: Opt. Express, 19, (2011) 5602.
[6] A. Joshi-Imre and S. Bauerdick: J Nanotechnol, 2014, (2014) 1.
[7] B. Radha and G. U. Kulkarni: Adv. Funct. Mater., 22, (2012) 2837.
[8] M. Deubel, G. von Freymann, M. Wegener, S. Pereira, K. Busch, and C. M. Soukoulis: Nat. Mater., 3, (2004) 444.
[9] X. Zhou, J. Liao, and P. Peng: Chin. J. Lasers, 48, (2021) 0802012.
[10] F. Clerici, M. Fontana, S. Bianco, M. Serrapede, F. Perrucci, S. Ferrero, E. Tresso, and A. Lamberti: ACS Appl. Mater. Interfaces, 8, (2016) 10459.
[11] M. Aminuzzaman, A. Watanabe, and T. Miyashita: J Nanopart Res, 12, (2010) 931.
[12] B. Kang, S. Han, J. Kim, S. Ko, and M. Yang: J. Phys. Chem. C, 115, (2011) 23664.
[13] D. Paeng, J. H. Yoo, J. Yeo, D. Lee, E. Kim, S. H. Ko,

and C. P. Grigoropoulos: Adv. Mater., 27, (2015) 2762.
[14] V. B. Nam, T. T. Giang, and D. Lee: Appl. Surf. Sci., 570, (2021) 151179.
[15] Y. Rho, K. T. Kang, and D. Lee: Nanoscale, 8, (2016) 8976.
[16] M. Hautefeuille, L. Cabriales, R. Pimentel-Dominguez, V. Velazquez, J. Hernandez-Cordero, L. Oropeza-Ramos, M. Rivera, M. P. Carreon-Castro, M. Grether, and E. Lopez-Moreno: Lab Chip, 13, (2013) 4848.
[17] V. B. Nam, J. Shin, A. Choi, H. Choi, S. H. Ko, and D. Lee: J. Mater. Chem. C, 9, (2021) 5652.
[18] E. Aparicio-Martinez, A. Ibarra, I. A. Estrada-Moreno, V. Osuna, and R. B. Dominguez: Sens. Actuators B Chem., 301, (2019) 127101.
[19] L. Torrisi, L. Silipigni, and G. Salvato: J. Mater. Sci. Mater. Electron., 31, (2020) 11001.
[20] X. Li, W. Feng, X. Zhang, S. Lin, Y. Chen, C. Chengwei, S. Chen, W. Wang, and Y. Zhang: Sens. Actuators B Chem., 321, (2020) 128483.
[21] V. B. Nam and D. Lee: Nanomaterials, 11, (2021) 576.
[22] X. Zhou, W. Guo, J. Fu, Y. Zhu, Y. Huang, and P. Peng: Appl. Surf Sci, 494, (2019) 684.
[23] N. Kurra, Q. Jiang, P. Nayak, and H. N. Alshareef: Nano Today, 24, (2019) 81.
[24] J. Kwon, H. Cho, H. Eom, H. Lee, Y. D. Suh, H. Moon, J. Shin, S. Hong, and S. H. Ko: ACS Appl. Mater. Interfaces, 8, (2016) 11575.
[25] S. H. Ko, H. Pan, D. Lee, C. P. Grigoropoulos, and H. K. Park: Jpn J Appl Phys, 49, (2010) 05EC03.
[26] P. Mueller, M. Thiel, and M. Wegener: Opt. Lett., 39, (2014) 6847.
[27] M. Hautefeuille, L. Cabriales, and R. Pimentel-Dominguez: Lab Chip, 13, (2013) 4848.
[28] M. Thiel, J. Fischer, G. von Freymann, and M. Wegener: Appl. Phys. Lett., 97, (2010) 221102.
[29] C. A. Rothenbach and M. C. Gupta: Opt Lasers Eng, 50, (2012) 900.
[30] E.-T. Hwu, H. Illers, W.-M. Wang, I.-S. Hwang, L. Jusko, and H.-U. Danzebrink: Rev. Sci. Instrum., 83, (2012) 013703.
[31] K. L. N. Deepak, R. Kuladeep, S. V. Rao, and D. N. Rao: Chem. Phys. Lett., 503, (2011) 57.
[32] T.-J. Chang, L. Vaut, M. Voss, O. Ilchenko, L. H. Nielsen, A. Boisen, and E.-T. Hwu: Commun. Phys., 4, (2021) 23.

(Received: August 1, 2023, Accepted: October 12, 2023)